Band Gap Control in an Active Elastic Metamaterial With Negative Capacitance Piezoelectric Shunting

Y. Y. Chen[1]
Department of Systems Engineering,
University of Arkansas at Little Rock,
Little Rock, AR 72204

G. L. Huang[1]
Department of Systems Engineering,
University of Arkansas at Little Rock,
Little Rock, AR 72204
e-mail: glhuang@ualr.edu

C. T. Sun
School of Aeronautics and Astronautics,
Purdue University,
West Lafayette, IN 47907
e-mail: sun@purdue.edu

Elastic metamaterials have been extensively investigated due to their significant effects on controlling propagation of elastic waves. One of the most interesting properties is the generation of band gaps, in which subwavelength elastic waves cannot propagate through. In the study, a new class of active elastic metamaterials with negative capacitance piezoelectric shunting is presented. We first investigated dispersion curves and band gap control of an active mass-in-mass lattice system. The unit cell of the mass-in-mass lattice system consists of the inner masses connected by active linear springs to represent negative capacitance piezoelectric shunting. It was demonstrated that the band gaps can be actively controlled and tuned by varying effective stiffness constant of the linear spring through appropriately selecting the value of negative capacitance. The promising application was then demonstrated in the active elastic metamaterial plate integrated with the negative capacitance shunted piezoelectric patches for band gap control of both the longitudinal and bending waves. It can be found that the location and the extent of the induced band gap of the elastic metamaterial can be effectively tuned by using shunted piezoelectric patch with different values of negative capacitance, especially for extremely low-frequency cases. [DOI: 10.1115/1.4028378]

Keywords: active acoustic metamaterials, band gap, negative effective spring, negative capacitance piezoelectric shunting

1 Introduction

Metamaterials are artificial materials engineered to produce properties, which may not be readily available in nature. The concept of a metamaterial was first proposed in the field of electromagnetics [1,2] and subsequently extended to the fields of acoustics and elastodynamics [3–6]. Acoustic and elastic metamaterials are structured materials that exhibit exceptional acoustic and elastic properties such as negative effective mass density and moduli. The core concept of the elastic/acoustic metamaterial is to use man-made microstructures (resonators) on a scale much less than the interrogating wavelength. A frequency regime around the resonance frequency, also called a band gap, was observed in the metamaterial, in which the wave cannot propagate through and is trapped in the resonators [7]. Acoustic and elastic metamaterials have a number of important applications including significant low-frequency sound/vibration attenuation [8,9], negative refraction [10,11], and acoustic/elastic lenses to focus sound/elastic waves [12,13]. At present, elastic metamaterials are mainly based on locally resonant mechanisms and can be interpreted by materials with single or double negative effective material constants such as negative effective mass density and bulk (shear) modulus [10,14,15]. Therefore, elastic metamaterials enlarge significantly the choice for material selection with a targeted application and provide a new way for manipulating elastic wave propagations.

However, the elastic metamaterials still face a big obstacle because of the limitation of the locally resonant mechanism. It was demonstrated that the forbidden gap from the current elastic metamaterial design is fixed and limited to a narrow frequency band. Moreover, the wave attenuation capability is significantly reduced if wave frequency is not close to the resonance frequency [16]. Recently, efforts to enlarge band gaps have been made in elastic metamaterials by varying physical parameters of internal multiresonators [17]. The width and position of the band gap can be tuned by adjusting the geometrical parameters of a Kagome-sphere lattice [18]. Pai [19] theoretically demonstrated that the longitudinal broadband wave absorption can be achieved in a bar structure with distributed absorbers related to different band gap frequency ranges in different sections [19]. However, this kind of broadband designs will increase the dimensions of the metamaterial and, moreover, can only be achieved passively. In many practical applications, dynamic loads and their frequency contents may vary with time and instantaneously changing microstructures/resonators in the metamaterial is extremely difficult.

Piezoelectric materials, which have the ability to convert mechanical energy into electrical energy and vice versa, are often used in active and passive vibration control applications [20,21]. When the piezoelectric material is strained, a charge develops across the element and energy is dissipated as current flows through an external electrical network or shunting. Apart from active techniques, passive ones consist in connecting a piezoelectric patch attached to the structure to a passive electric network, in which the energy generated by the piezoelectric patches is consumed within the external circuit. Forward [22] was the first to investigate adding a resonant, or resistive–inductive, shunt to a piezoelectric actuator to damp a specific mode of vibration of a system. A resonant shunt works as a means of vibration control by cancelling the capacitive reactance of the electrical domain at a specific frequency to increase the damping of the system. Hagood and von Flotow [23] extended Forward's research with the development of an equation and indicated that a resonant shunt introduces another degree of freedom to the system. Therefore, the resonant shunt acts as a narrow-band vibration absorber. Based on this principle, electrical control of elasticity was performed in

[1]Present address: Department of Mechanical and Aerospace Engineering, University of Missouri-Columbia, MO 65211.

Contributed by the Technical Committee on Vibration and Sound of ASME for publication in the Journal of Vibration and Acoustics. Manuscript received October 12, 2013; final manuscript received July 31, 2014; published online September 11, 2014. Assoc. Editor: Jiong Tang.

piezoelectric polymer films and piezoelectric stack transducers by connecting an electric circuit parallel to the sample electrodes [24]. Experimental observations of the characteristics of the dynamic elastic constant agreed well with these theoretical predictions. Airold and Ruzzene [25] used multiresonant shunts to generate multiple local resonant band gaps in a beam. Subsequently, they proposed the design of one dimensional tunable acoustic metamaterial through periodic arrays of resonance shunted piezos. It was demonstrated that the resonance frequencies can be conveniently tuned through proper selection of the electrical impedance connected to each patch, so that no modification to the structure is necessary. The resonant shuts were also applied in acoustic wave attenuation, where a reduced-order model was developed to solve the fully coupled electromechanical acoustic system [26]. Periodic arrays of negative capacitance shunted piezoelectric patches were employed and demonstrated numerically by employing transfer matrix method to control the band gaps of phononic beams [27]. These studies demonstrated how piezoelectric shunting patches can be utilized to affect the equivalent mechanical properties of an elastic waveguide and therefore suggest their applications in developing tunable band gaps in phononic crystals. In addition, a 1D active acoustic metamaterial with simultaneously programmable bulk modulus and density was proposed through mounting voltage controlled piezoelectric panels on the face and side wall of the cavity [28]. However, designing active elastic metamaterials for tuning resonant microstructures by using piezoelectric shunting patches has not been comprehensively investigated yet. It is believed that active elastic metamaterials can achieve a much wider range of effective parameters than their passive counterparts by introducing additional degree of freedom in controlling them independently.

In the study, the concept of a new active elastic metamaterial is first proposed to achieve band gap control through the use of negative capacitance shunted piezoelectric patches. An active mass-in-mass lattice system with the inner spring connected to the negative capacitance piezoelectric shunting is studied to demonstrate the flexible band gap control mechanism over a wide frequency range. This promising application is then demonstrated with an active elastic metamaterial plate integrated with negative capacitance shunted piezoelectric patches for longitudinal and bending waves. The result reveals that using negative capacitive shunting to tune the band gap is very effective, although improvements can be further made at this point.

2 Band Gap Control in Active Elastic Metamaterials

2.1 Negative Capacitance Piezoelectric Shunting. A single piezoelectric patch shunted with negative capacitance circuits have been used for multimode damping of a beam structure [29,30]. By following the similar principle, Beck et al. performed an experimental analysis of a cantilever beam with a negative capacitance shunted piezoelectric periodic array [31]. The results showed that such structure can be an effective global vibration reduction system. On the other hand, it has been experimentally demonstrated that the elasticity of piezoelectric materials shunted with negative capacitance circuits can be electrically tuned [32,33]. Figure 1 shows the circuit that influences/controls the elastic parameters of the piezoelectric sample, designated as gyrator circuit A. It consists of a capacitor, a potentiometer and an operational amplifier (OA). A piezoelectric sample disconnected from the circuit is shown in Fig. 1(*a*). A static stress is applied to this sample, which induces voltage V_p, and the capacitance of the piezoelectric element is denoted as C_p for open circuit. The magnitude of strain polarization is shown by the length of the arrow. The polarization induces negative charge on the upper electrode, and positive charge on the lower electrode. When the piezoelectric sample is connected to the circuit, as shown in Fig. 1(*b*), the noninverting and inverting of the OA are V_{in}^{+} and V_{in}^{-}, respectively.

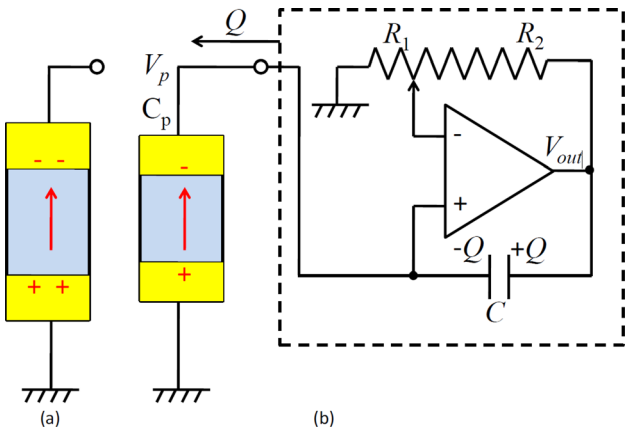

Fig. 1 Principle of operation of the negative capacitance circuit A, (*a*) piezoelectric sample disconnect from the circuit and (*b*) piezoelectric sample connected with the circuit

Through straightforward circuit analysis, the equivalent capacitance of this circuit is determined as

$$-C_n = -\frac{R_1}{R_2}C \tag{1}$$

where C_n is always a positive value.

This circuit can be considered as a negative capacitance circuit with a capacitance $-C_n$ to increase or decrease the elastic properties. Stable operation of the negative feedback circuit requires the condition $C_n < C_p$ for the circuit A. Another type of negative capacitance circuit denoted as circuit B, which decreases the elastic properties, is that the sample electrode is connected to the inverting input of the OA, and Eq. (1) holds for this circuit also, and the stability condition requires $C_n > C_p$. Equation (1) shows that any negative capacitance can be obtained by appropriately selecting the circuit parameters. Moreover, different tunings can be performed by simply varying one potentiometer of the synthetic circuit.

Now consider a thin, shunted piezoelectric patch connected to a parallel negative capacitance $-C_n$, which is schematically illustrated in Fig. 2(*a*). It is readily found that the shunted system is equivalent to a "simple" transducer with a lower capacitance, as shown in Fig. 2(*b*).

Indeed, the total electrical charge Q_t flowing in the system is given by

$$Q_t = Q_p - C_n V \tag{2}$$

and, from Eq. (2), the equivalent system is governed by the constitutive relation in Laplace domain when the piezoelectric element is loaded uniaxially along the 1 axis as

$$\begin{bmatrix} I \\ \sum_{11} \end{bmatrix} = \begin{bmatrix} s(C_p - C_n) & sd_{31}A \\ d_{13}/h & s_{11} \end{bmatrix} \begin{bmatrix} V \\ E_{11} \end{bmatrix} \tag{3}$$

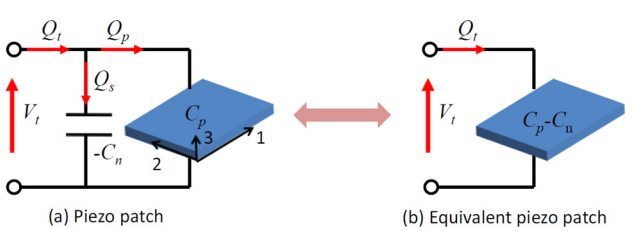

Fig. 2 (*a*) Piezoelectric patch connected to a parallel negative capacitance $-C_n$ and (*b*) equivalent piezoelectric patch

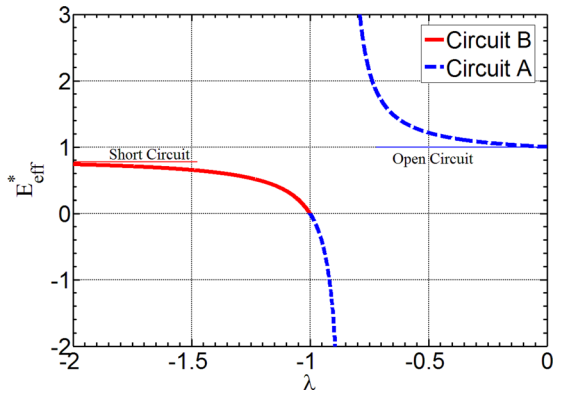

Fig. 3 Normalized effective modulus of piezoelectric patch with different NCRs in circuits A and B, respectively

where $s = i\omega$ is the Laplace operator, $C_p = (\varepsilon_{33}A/h)$, ε_{33} is the dielectric constant of the material, d_{31} is the piezoelectric constants, s_{11} is the compliance matrix of the piezoelectric patch, $\sum_{11}$ and E_{11} are stress and strain along 1 axis direction, A and h are the electrode area and thickness of the piezoelectric patch, respectively, the 1 axis is the direction of the length of the lead zirconate titanate (PZT) patch, the 3 axis is the direction of the thickness of the patch, and the 2 axis is perpendicular to both the 1 and 3 axes, as shown in Fig. 2(*a*). According to Hagood and von Flotow [23], modified effective Young's modulus of the shunted patch can be expressed according to the following expression, which is independent of frequency ω, as

$$E_p^{SU} = E_p^E \frac{C_p^T - C_n}{C_p^T(1 - k_{31}^2) - C_n} \tag{4}$$

where $k_{31} = d_{31}/\sqrt{s_{11}\varepsilon_{33}}$ denotes the electromechanical coupling coefficient, E_p^E is Young's modulus of the piezoelectric material when the shunting network is in a short circuit configuration, $C_p^T = C_p$ is the electrical capacitance of the piezoelectric material at constant stress. The relationship between the open circuit Young's modulus and short circuit Young's modulus is

$$E_p^E = E_p^D(1 - k_{31}^2) \tag{5}$$

A significant result from Eq. (4) is that the shunt has the ability to modify elastic properties, and thus may be used to control the dynamic behavior of the piezoelectric material.

Figure 3 shows the normalized effective modulus $E^*_{eff} = E_p^{SU}/E_p^D$ of PZT-5H in function of the negative capacitance ratio (NCR), which is defined as $\lambda = -(C_n/C_p)$. The decrease of the effective modulus is corresponding to the negative capacitance circuit A and B, as shown in Fig. 1(*a*), and the increase of the effective modulus is related to the negative capacitance circuit A. It can be found that the normalized effective stiffness modulus is equal to the short circuit stiffness for large values of λ and equal to the open circuit stiffness for small values of λ. For λ equals to -1.0, the effective modulus becomes zero. For λ near unity, the normalized effective modulus exhibits an asymptotic behavior. When λ approaches to $-(1 - k_{31}^2)$ from positive small values, the effective modulus approaches positive infinity (dash line). However, when λ approaches to $-(1 - k_{31}^2)$ from large negative values, the effective modulus is changed from a positive value to a negative value, and eventually approaches negative infinity. The tunable modulus behavior of the shunted piezoelectric element will be used for the concept design of the active elastic metamaterial.

2.2 Active Mass-in-Mass System. The one-resonator mass-in-mass model has been proposed by Huang et al. [5] to interpret the effective mass density of the one-dimensional elastic metamaterial. In this study, we will consider the same one-dimensional lattice consisting of active mass-in-mass units as shown in Fig. 4. The unit-cells are placed periodically at a spacing of L. The two rigid masses are denoted as m_1 and m_2, respectively. The two spring constants k_1 and k_2 represent the interactions among the masses. Note that, in each unit cell, the inner spring constant with the negative capacitance piezoelectric shunting is denoted as $k_2(\lambda) = (E_p^{SU}A_p/l_p)$, which is a function of NCR λ, where A_p and l_p are the cross-sectional area and length of the piezoelectric patch, respectively. Combining with Eq. (4), the relationship of the stiffness and the capacitance of the piezoelectric transducer can be established.

For harmonic wave propagation in the mass-in-mass lattice system, the equations of motion for the jth unit cell can be expressed as

$$m_1 \frac{d^2u_1^{(j)}}{dt^2} + k_1\left(2u_1^{(j)} - u_1^{(j-1)} - u_1^{(j+1)}\right) + k_2(\lambda)\left(u_1^{(j)} - u_2^{(j)}\right) = 0 \tag{6}$$

$$m_2 \frac{d^2u_2^{(j)}}{dt^2} + k_2(\lambda)\left(u_2^{(j)} - u_1^{(j)}\right) = 0 \tag{7}$$

where $u_\alpha^{(j)}$ represents the displacement of mass "α" in the jth cell. The harmonic wave form of the displacement at the jth cell is

$$u_\alpha^{(j)} = B_\alpha e^{i(qx - \omega t)} \tag{8}$$

where B_α is the complex wave amplitude, q is the wave number, and $\alpha = 1$ and 2 denoting the two masses. Substitution of Eq. (8) into Eqs. (6) and (7) yields two homogeneous equations from which the dispersion equation can be obtained as

$$m_1m_2\omega^4 - [(m_1 + m_2)k_2(\lambda) + 2m_2k_1(1 - \cos(qL))]\omega^2 + 2k_1k_2(\lambda)(1 - \cos(qL)) = 0 \tag{9}$$

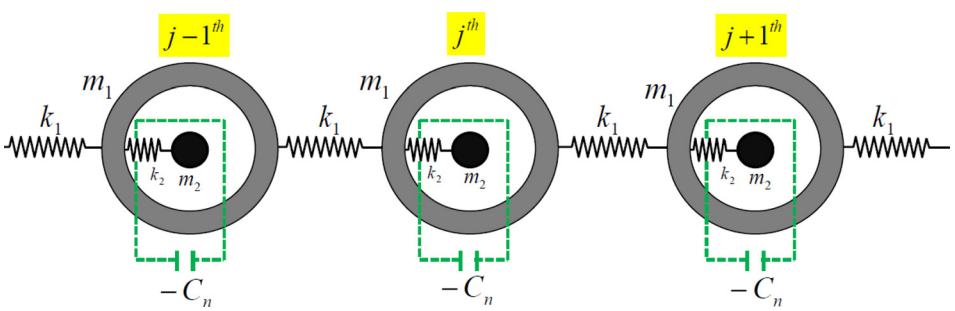

Fig. 4 Active mass-in-mass lattice system with inner spring to represent negative capacitance piezoelectric shunting

It is evident that the dispersion curves (the plots of ω versus qL), of the resonator system are influenced by a number of parameters including the effective modulus $k_2(\lambda)$.

In this study, wave band gaps in the active mass-in-mass system are investigated for different active spring constant values. Attention is focused on the roles played by the active spring parameter $k_2(\lambda)$ which is function of the NCR $\lambda = -(C_n/C_p)$.

The variation of band gap corresponding to different NCRs is shown in the shaded regions in Fig. 5. In the example, $m_2/m_1 = 9$, $k_1 = 10^8\,\mathrm{N/m}$, and the inner effective spring k_2 is calculated from the longitudinal deformation in the shunted piezoelectric (PZT-5H) beam. The material properties and dimensions of the piezoelectric patch are $\varepsilon_{33} = 3.10 \times 10^{-8}\,\mathrm{F/m}$, $d_{31} = -2.74 \times 10^{-10}\,\mathrm{C/m^2}$, $E_P = 60.6$ GPa, and $A_p/l_p = 74.6 \times 10^{-6}\,\mathrm{m}$. In the case, the effective stiffness of piezoelectric material with open circuit is represented by $k_2(\lambda = 0) = 4.46 \times 10^6\,\mathrm{N/m}$ with $k_2(0)/k_1 = 0.0446$. In the figures, $\omega_0 = \sqrt{k_2(0)/m_2}$ is the local resonance frequency of the resonator system with the open circuit. Figure 5(*a*) shows the band gap when $\lambda = 0$, i.e., the shunting circuits are open. The band gap is in the range of $\omega = \omega_0$–$3.2\omega_0$. The effective modulus of shunted PZT patch will change with the change of the value of connected negative capacitances, which induces band gap changes in the elastic metamaterial. Figure 5(*b*) shows the band gap of the elastic metamaterial when $\lambda = -0.8$ and the spring stiffness ratio $k_2(-0.8)/k_1$ increases. Comparing the two diagrams, it is found that the width of the band gap is slightly enlarged, and the band gap range is shifted from the original (ω_0–$3.2\omega_0$) to ($1.8\omega_0$–$5.9\omega_0$) as shown in Fig. 5(*b*). Figure 5(*c*) shows the band gap of the elastic metamaterial when $\lambda = -0.84$ and the spring stiffness ratio become significantly large. The width of new band gap is significantly enlarged from the original (ω_0–$3.2\omega_0$) to ($3.6\omega_0$–$12.4\omega_0$). Therefore, the broadband frequency of the stop band could be tuned to be (ω_0–$12.4\omega_0$) by the active elastic metamaterial connecting to different negative capacitances such as $\lambda = 0$, $\lambda = -0.8$, and $\lambda = -0.84$. Figures 5(*d*) and 5(*e*) show the band structure diagrams of the active elastic metamaterial when $\lambda = -0.9$ and $\lambda = -1.0$, for which the spring stiffness ratio becomes negative and zero, respectively. In these two cases, the local resonance mechanism in the metamaterial is totally absent. The elastic metamaterial now functions as the conventional material and the low-frequency stop band disappears. When the NCR reduces further from $\lambda = -1.0$, the effective spring stiffness increases from zero to the value of the piezoelectric materials

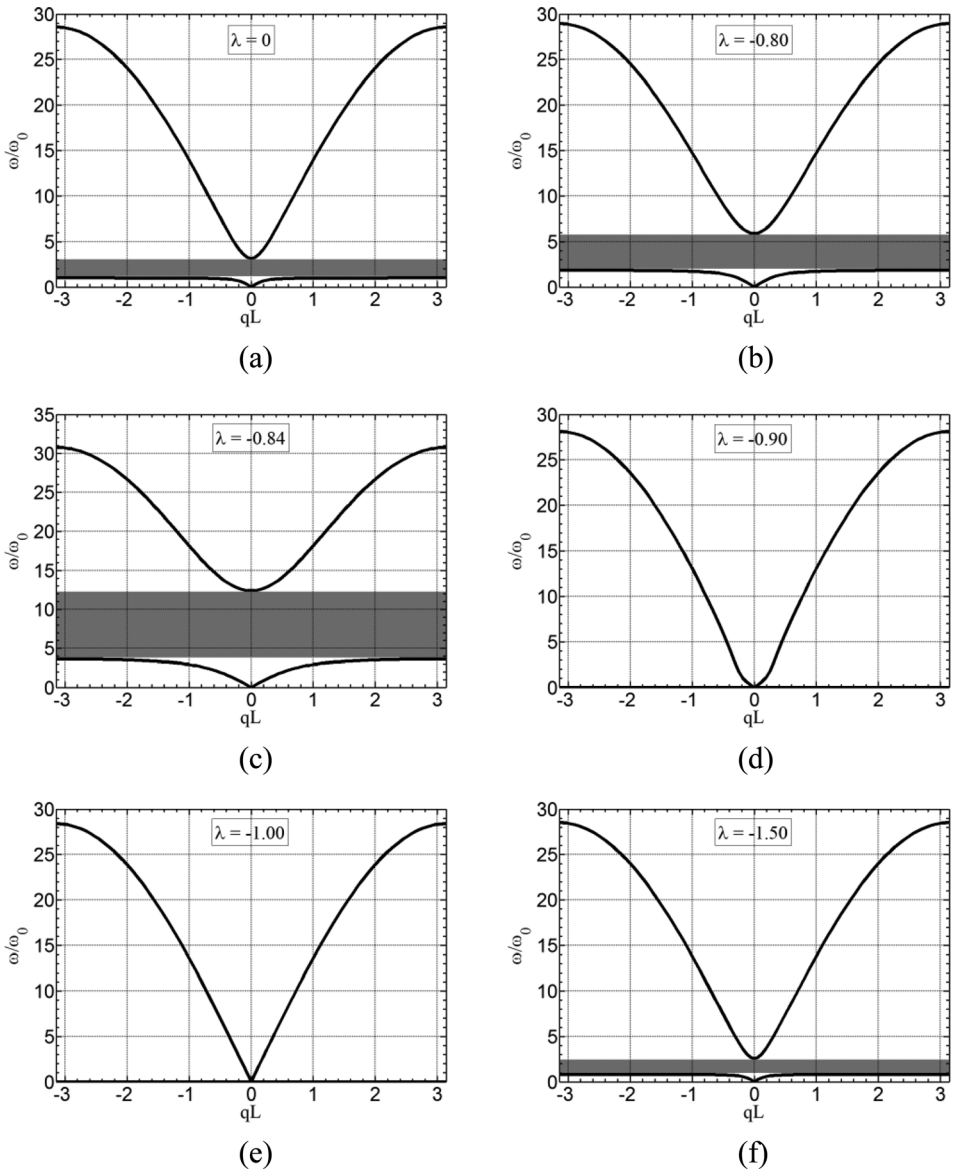

Fig. 5 Band gap of the active mass-in-mass lattice system with different NCRs, (*a*) $\lambda = 0$, (*b*) $\lambda = -0.80$, (*c*) $\lambda = -0.84$, (*d*) $\lambda = -0.90$, (*e*) $\lambda = -1.00$, and (*f*) $\lambda = -1.50$

with short circuits. Figure 5(*f*) shows the band structure diagram of the elastic metamaterial when $\lambda = -1.5$, in which the spring stiffness ratio becomes positive again with $k_2(-1.5)/k_1 = 0.006$. It is expected that the lower frequency band gap can be achieved in the range of $(0.8\omega_0$–$2.6\omega_0)$. If NCR reduces further from $\lambda = -1.5$, the band gap will not change significantly.

To interpret the wave propagation and attenuation mechanism of the active elastic metamaterial with different NCRs, the displacement ratio of the two masses is also plotted in the Fig. 6, which can be analytically determined as $(U_2/U_1) = k_2(\lambda)/(-m_2\omega^2 + k_2(\lambda))$. It can be found that the stop band is caused by out of phase motion between mass 1 and mass 2. When $k_2(\lambda)$ becomes negative, the two masses will always move in the same phase, therefore, no stop band can be observed at this case. When k_2 becomes zero, the inner mass is motionless and wave propagation behavior will be the same as the wave propagation in single mass-spring $(m_1 - k_1)$ system.

For the discrete model, the lower bond frequency of the band gap, which is equal to the resonance frequency of m_2 [5], can be determined as

$$\omega_{\mathrm{L}} = \sqrt{\frac{k_2(\lambda)}{m_2}} \tag{10}$$

The upper bond frequency of the band gap can be determined from the dispersion relations of Eq. (9) at the cutoff frequency with $qL = 0$ as

$$\omega_{\mathrm{U}} = \sqrt{\frac{(m_1 + m_2)k_2(\lambda)}{m_1 m_2}} \tag{11}$$

Finally, the general variations of band gaps of the elastic metamaterial are shown in the shaded region in Fig. 7. In the figure, the solid red line represents the upper bound of the stop band, and the dashed blue line is the lower bound of the stop band. When the shunted piezoelectric NRC λ approaches -1.0 from negative infinity, the width of band gap of the elastic metamaterial will gradually decrease from the range $(\omega_0$–$2.8\omega_0)$ to zero. When λ is tuned from -1.0 to $-\left(1 - k_{31}^2\right)$, the elastic metamaterial will become a conventional material and the stop band disappears. Similarly, when the value of λ is changed from $-\left(1 - k_{31}^2\right)$ to 0 (open circuit), one can find that the location and bandwidth of band gaps are also distinctly changed. The bandwidth of stop band of the elastic metamaterial will greatly reduce from a large bandwidth to normal metamaterial band gap range $(\omega_0$–$3.2\omega_0)$. The result of the active elastic metamaterial provides a very promising solution to overcome the obstacle in the elastic metamaterial and the location and the width of band gaps are actively tuned.

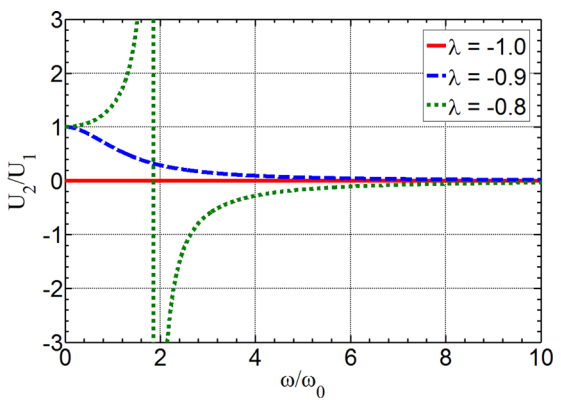

Fig. 6 Displacement amplitude ratio U_2/U_1 of the inner mass m_2 to the outer mass m_1

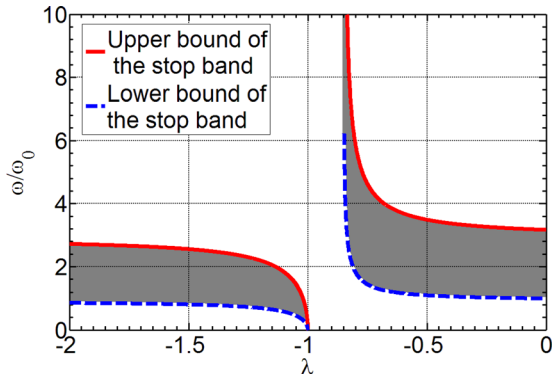

Fig. 7 Band gap variations of the active mass-in-mass lattice system with different NCRs (bond should be bound)

2.3 Band Gap Control in Active Elastic Metamaterial Plate. A thin metamaterial plate with periodic cantilever-mass microstructures was proposed for low-frequency band gap applications for both in-plane and out-of-plane waves [16,34]. The low-frequency band gaps in the elastic metamaterial plate were investigated numerically and experimentally. In this study, we illustrate the practical application of how the periodic array of shunting piezoelectric patches bonded to the cantilever beam can function as the building block of an active elastic metamaterial. Effective modulus of such resonant unit can be numerically characterized by integrating the metamaterial plate with the shunting piezoelectric patch with different negative capacitances. Therefore, the local resonance frequencies of the metamaterial plate can be conveniently tuned through the proper selection of the electrical negative capacitance connected to each patch without modifying the microstructure.

Figure 8(*a*) shows the active elastic metamaterial plate with a periodic array of cantilever-masses bonded by shunted piezoelectric patches. The detailed microstructure in the unit cell is shown in Fig. 8(*b*). The plate behaves as a one-dimensional waveguide that supports the propagation of axial and transverse waves. In the low-frequency range, the behavior of the waveguide of the

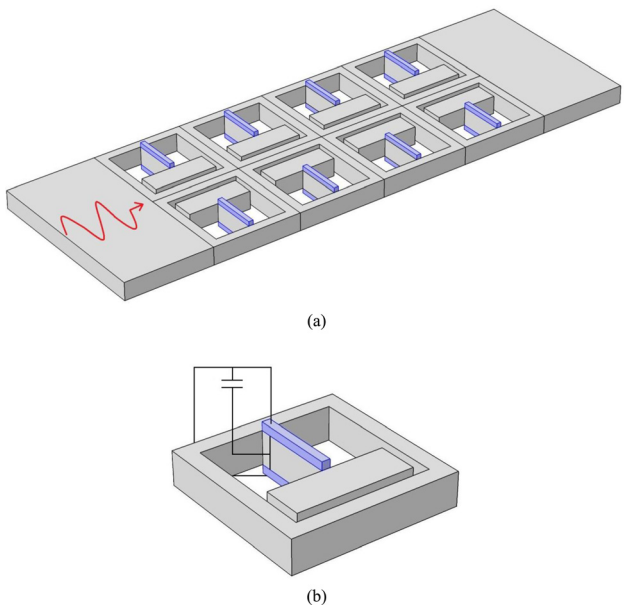

Fig. 8 (*a*) Active elastic metamaterial plate with a periodic array of the cantilever-mass system bonded by shunted piezoelectric patches and (*b*) detailed microstructure in the unit cell

resonators can be conveniently described through the Euler–Bernoulli theory with piecewise elastic and mass properties. The negative capacitance shunts are applied to piezoelectric patches installed in a periodic array, which consists of a series of equally spaced piezoelectric patches.

The thin plate beam is made of stainless steel ($E_s = 195$ GPa, $\rho_s = 8000$ kg/m^3, and $\upsilon_s = 0.33$) with thickness $t_s = 1$ mm and width $b_s = 0.45$ mm. The shunted piezoelectric materials are PZT-5H ($E_p = 60.6$ GPa, $\rho_p = 7500$ kg/m^3, and $\upsilon_p = 0.34$) with thickness $t_p = 0.1$ mm, length $l_p = 2.7$ mm, and width $b_p = 0.45$ mm. The spacing of the adjacent unit cells is $a = 5.6$ mm. Due to the geometric complexity of the microstructure, the finite element technique is employed with the aid of the commercial finite element software, ANSYS v13.0 to determine the band diagram of the active elastic metamaterial. In the numerical simulation, 3D solid element SOLID45 is chosen to model the thin steel plate and piezoelectric patches with effective modulus (based on the connected negative capacitance), and five elements are used in the thickness direction. Manual mesh strategy is used to better control mesh density and element shape for the complex interior cantilever-mass geometry. The effective bending stiffness of the embedded composite cantilever beam can be determined as

$$D_b = \frac{E_p^{SU} b_p t_p^3}{6} + \frac{E_p^{SU} b_p t_p (t_p + t_c)^2}{2} + \frac{E_c b_c t_c^3}{12} \quad \text{for bending wave} \tag{12}$$

$$D_l = \frac{E_p^{SU} b_p t_p^3}{6} + \frac{E_c b_c t_c^3}{12} \quad \text{for longitudinal wave} \tag{13}$$

from which the effective Young's modulus of the composite beam can be determined and will be used in the finite element analysis. Based on Eqs. (4), (12), and (13), the relationship of the plate stiffness and the capacitance of the piezoelectric transducer can be established. The dispersion relations of the active elastic metamaterial plates with surface-bonded the piezoelectric patches with different negative capacitance for in-plane extensional wave are plotted in Fig. 9. Attention is focused on the first band gap variation (identified in the shaded regions) with different NCRs $\lambda = -(C_n/C_p)$. The normalized wave number is defined as qa. Figure 9(*a*) shows the dispersion diagram and the first band gap when $\lambda = 0$, i.e., the shunting circuits are open. In the figures, $\omega_0 = \sqrt{k_{eff}/m_2}$ is the local resonance frequency of the cantilever resonator system with the open circuits for $k_{eff} = D_l/3l_p^3$. The

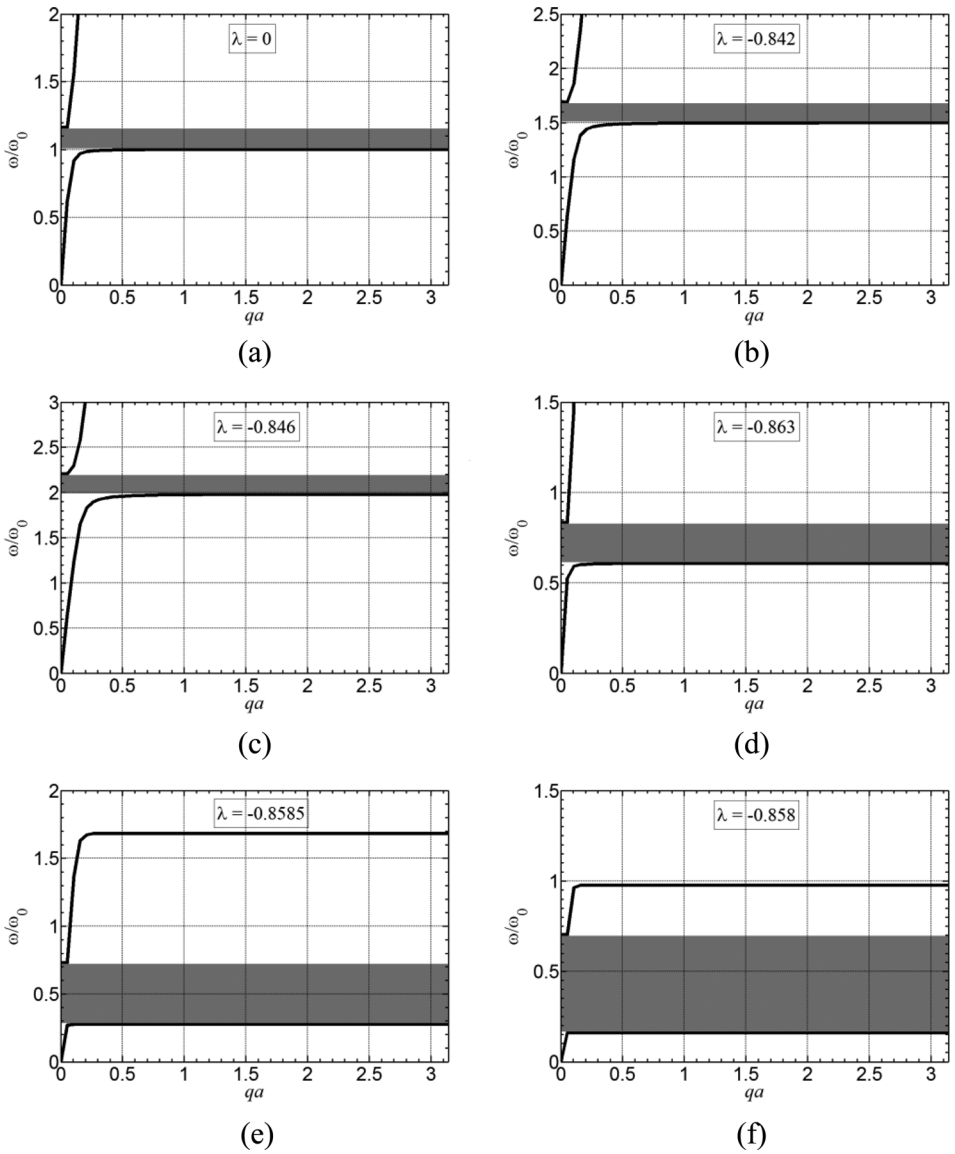

Fig. 9 Band gap variation of the active elastic metamaterial plate with different NCRs for in-plane longitudinal wave, (*a*) $\lambda = 0$, (*b*) $\lambda = -0.842$, (*c*) $\lambda = -0.846$, (*d*) $\lambda = -0.863$, (*e*) $\lambda = -0.8585$, and (*f*) $\lambda = -0.858$

band gap of the open shunting circuit is in the range of $\omega = \omega_0$–$1.18\omega_0$. The effective bending stiffness of the cantilever beam with the shunted PZT patch will change with the change of value of the connected negative capacitance, which induces the frequency range and bandwidth of the first band gap in the active elastic metamaterial plate. Figure 9(*b*) shows the dispersion diagram and the first band gap of the elastic metamaterial plate when $\lambda = -0.842$, in which the effective stiffness of the shunted piezoelectric patch increases as a positive value; therefore, the effective bending stiffness of the cantilever beam will be increased. Comparing the band diagram with the open circuit, it is found that the band gap is shifted from the original band gap (ω_0–$1.2\omega_0$) to ($1.5\omega_0$–$1.7\omega_0$) as shown in Fig. 9(*b*). However, the bandwidth of the stop band is not enlarged at this case. Figure 9(*c*) shows the band gap of the elastic metamaterial plate when $\lambda = -0.846$, in which the effective modulus of the composite beam becomes larger. The new band gap is observed to continuously shift to ($1.98\omega_0$–$2.2\omega_0$). Therefore, the stop band of the metamaterial plate could be tuned by changing the connected negative capacitance in a small value around the piezoelectric capacitance. Figure 9(*d*) shows the band structure diagram and the first band gap of the elastic metamaterial plate when $\lambda = -0.863$, in which the effective stiffness of the shunted piezoelectric patch becomes a negative value, and therefore the effective bending stiffness of the cantilever beam will be decreased. Comparing the band diagram with the open circuit, it is found that the band gap is lowered from the original band gap (ω_0–$1.2\omega_0$) to ($0.61\omega_0$–$0.84\omega_0$). Figures 9(*e*) and 9(*f*) show the band structure diagram and the first band gap of the elastic metamaterial plate when $\lambda = -0.8585$ and $\lambda = -0.85$, respectively, in which the effective stiffness of the shunted piezoelectric patch is reduced further in a negative value. It can be found that the extreme low-frequency band gaps can be observed at range of ($0.27\omega_0$–$0.73\omega_0$) and ($0.16\omega_0$–$0.7\omega_0$) for both cases. It is also interesting to notice that the width of the stop band becomes wider and is very sensitive to the change of the negative capacitance. The high sensitive negative capacitance can be accomplished through a specific circuit design, which is the ongoing research.

Figure 10 shows the band gap variation (identified in the shaded regions) of the active elastic metamaterial plate with surface-bonded piezoelectric patches with different NCRs $\lambda = -(C_n/C_p)$ for the out-of-plane bending wave. Figure 10(*a*) shows the band

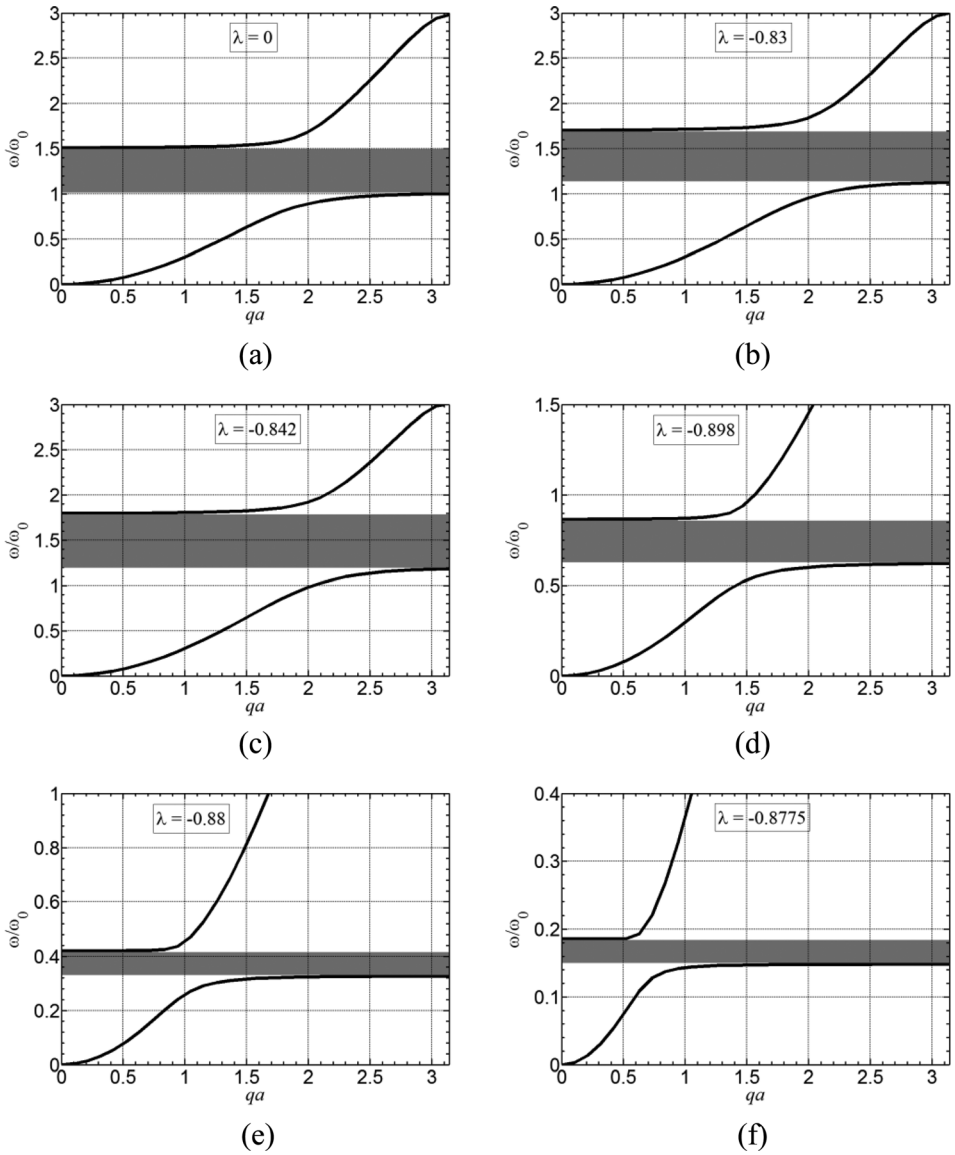

Fig. 10 Band gap variation of the active elastic metamaterial plate with different NCRs for out-of-plane bending wave, (*a*) $\lambda = 0$, (*b*) $\lambda = -0.83$, (*c*) $\lambda = -0.842$, (*d*) $\lambda = -0.898$, (*e*) $\lambda = -0.88$, and (*f*) $\lambda = -0.8775$

gap when $\lambda = 0$, i.e., the shunting circuits are open. In the figures, $\omega_0 = \sqrt{k_{\text{eff}}/m_2}$ is the local resonance frequency of the cantilever resonator system with the open circuit with $k_{\text{eff}} = D_b/3l_p^3$. The first band gap is in the range of $\omega = \omega_0$–$1.5\omega_0$. Figure 10(*b*) shows the dispersion diagram and the first band gap of the elastic metamaterial plate when $\lambda = -0.83$, in which the effective modulus of the shunted piezoelectric patch increases in a positive value, therefore the bending stiffness of the cantilever beam is increased. The width of the band gap is almost not changed; however, the frequency range of the first band gap is shifted from the original (ω_0–$1.5\omega_0$) to ($1.13\omega_0$–$1.7\omega_0$). Figure 10(*c*) shows dispersion diagram and the first band gap of the elastic metamaterial plate when $\lambda = -0.842$, in which the effective stiffness of the shunted piezoelectric patch continuously increases in a positive value. The first band gap is shifted from the original band gap (ω_0–$1.5\omega_0$) to ($1.19\omega_0$–$1.8\omega_0$). However, if the effective stiffness of the shunted piezoelectric patch continuously increases to a larger value, the local resonance is hard to be induced in the cantilever beam in the low-frequency range because of the finite stiffness in the host medium. Figure 10(*d*) shows the band structure diagram of the elastic metamaterial plate when $\lambda = -0.898$, in which the effective modulus of the shunted piezoelectric patch becomes a negative value, and therefore the effective bending stiffness of the cantilever beam is decreased. Comparing the band diagram with the open circuit, it is found that the band gap is shifted from the original band gap (ω_0–$1.5\omega_0$) to ($0.62\omega_0$–$0.87\omega_0$). Figures 10(*e*) and 10(*f*) show the band structure diagram of the elastic metamaterial plate when $\lambda = -0.88$ and $\lambda = -0.8775$, respectively, in which the effective stiffness of the shunted piezoelectric patch is further reduced in a negative value. It is seen that the extremely low-frequency band gaps are located at the ranges of ($0.33\omega_0$–$0.42\omega_0$) and ($0.15\omega_0$–$0.19\omega_0$) for both cases. However, the width of the stop band becomes very narrow at the low-frequency cases for the bending wave. One important requirement to achieve the tunable band gap is to have the ability to adjust the value of the negative capacitance very accurately.

3 Summary

In the study, we first investigated dispersion curves and band gap control in an active mass-in-mass lattice system. The unit cell of the lattice system consists of inner masses connected by active linear springs to represent negative capacitance piezoelectric shunting. It was demonstrated that the band gaps can be actively controlled and tuned by varying the effective spring constant through applying negative capacitance. Subsequently, this technique is implemented in the active elastic metamaterial plate with periodically surface-bonded piezoelectric patches which are shunted with a negative capacitive circuit. It is demonstrated that the location and the range of induced band gap of the active elastic metamaterial plate can be effectively tuned by using shunted piezoelectric patches with different NCRs, especially for extremely low-frequency cases.

Acknowledgment

This work was supported by the Air Force Office of Scientific Research under Grant No. AF 9550-10-0061 with Program Manager Dr. Byung-Lip (Les) Lee.

References

[1] Pendry, J. B., Holden, A. J., Robbins, D. J., and Stewart, W. J., 1999, "Magnetism From Conductors and Enhanced Nonlinear Phenomena," IEEE Trans. Microwave Theory Tech., **47**(11), pp. 2075–2084.
[2] Smith, D. R., Padilla, W. J., Vier, D. C., Nemat-Nasser, S. C., and Schultz, S., 2000, "Composite Medium With Simultaneously Negative Permeability and Permittivity," Phys. Rev. Lett., **84**(18), pp. 4184–4187.
[3] Liu, Z. Y., Chan, C. T., and Sheng, P., 2005, "Analytic Model of Phononic Crystals With Local Resonances," Phys. Rev. B, **71**(1), p. 014103.
[4] Fang, N., Xi, D., Xu, J., Ambati, M., Srituravanich, W., Sun, C., and Zhang, X., 2006, "Ultrasonic Metamaterials With Negative Modulus," Nature Mater., **5**(6), pp. 452–456.
[5] Huang, H. H., Sun, C. T., and Huang, G. L., 2009, "On the Negative Effective Mass Density in Acoustic Metamaterials," Int. J. Eng. Sci., **47**(4), pp. 610–617.
[6] Yao, S. S., Zhou, X. N., and Hu, G. K., 2008, "Experimental Study on Negative Effective Mass in a 1D Mass–Spring System," New J. Phys., **10**(4), p. 043020.
[7] Liu, Z., Zhang, X., Mao, Y., Zhu, Y. Y., Yang, Z., Chan, C. T., and Sheng, P., 2000, "Locally Resonant Sonic Materials," Science, **289**(5485), pp. 1734–1736.
[8] Yang, Z., Mei, J., Yang, M., Chan, N. H., and Sheng, P., 2008, "Membrane-Type Acoustic Metamaterial With Negative Dynamic Mass," Phys. Rev. Lett., **101**(20), p. 204301.
[9] Mei, J., Ma, G., Yang, M., Yang, Z., Wen, W., and Sheng, P., 2012, "Dark Acoustic Metamaterials as Super Absorbers for Low-Frequency Sound," Nat. Commun., **3**, p. 756.
[10] Liu, X. N., Hu, G. K., Huang, G. L., and Sun, C. T., 2011, "An Elastic Metamaterial With Simultaneously Negative Mass Density and Bulk Modulus," Appl. Phys. Lett., **98**(25), p. 251907.
[11] Christensen, J., and Abajo, F. J. G., 2012, "Negative Refraction and Backward Waves in Layered Acoustic Metamaterials," Phys. Rev. B, **86**(2), p. 024301.
[12] Lin, S. S., Tittmann, B. R., and Huang, T. J., 2012, "Design of Acoustic Beam Aperture Modifier Using Gradient-Index Phononic Crystals," J. Appl. Phys., **111**(12), p. 123510.
[13] Yan, X., Zhu, R., Huang, G. L., and Yuan, F. G., 2013, "Focusing Guided Waves Using Surface Bonded Elastic Metamaterials," Appl. Phys. Lett., **103**(12), p. 121901.
[14] Wu, Y., Lai, Y., and Zhang, Z. Q., 2011, "Elastic Metamaterials With Simultaneously Negative Effective Shear Modulus and Mass Density," Phys. Rev. Lett., **107**(10), p. 105506.
[15] Lai, Y., Wu, Y., Sheng, P., and Zhang, Z. Q., 2011, "Hybrid Elastic Solids," Nature Mater., **10**(8), pp. 620–624.
[16] Huang, H. H., and Sun, C. T., 2009, "Wave Attenuation Mechanism in an Acoustic Metamaterial With Negative Effective Mass Density," New J. Phys., **11**(1), p. 013003.
[17] Zhu, R., Liu, X. N., Hu, G. K., Sun, C. T., and Huang, G. L., 2013, "An Chiral Elastic Metamaterial Beam for Broadband Vibration Suppression," J. Sound Vib., **333**(10), pp. 2759–2773.
[18] Liu, Y., Sun, X. Z., Jiang, W. Z., and Gu, Y., 2014, "Tuning of Bandgap Structures in Three-Dimensional Kagome-Sphere Lattice," ASME J. Vib. Acoust., **136**(2), p. 021016.
[19] Pai, P. F., 2010, "Metamaterial-Based Broadband Elastic Wave Absorber," J. Intell. Mater. Syst. Struct., **21**(5), pp. 517–528.
[20] Tang, J., and Wang, K. W., 1999, "Vibration Control of Rotationally Periodic Structures Using Passive Piezoelectric Shunt Networks and Active Compensation," ASME J. Vib. Acoust., **121**(3), pp. 379–390.
[21] Tang, J., and Wang, K. W., 2001, "Active-Passive Hybrid Piezoelectric Networks for Vibration Control: Comparisons and Improvement," Smart Mater. Struct., **10**(4), pp. 794–806.
[22] Forward, R. L., 1979, "Electronic Damping of Vibrations in Optical Structures," J. Appl. Opt., **18**(5), pp. 690–697.
[23] Hagood, N. W., and Flotow, A. V., 1991, "Damping of Structural Vibrations With Piezoelectric Materialsand Passive Electrical Networks," J. Sound Vib., **146**(2), pp. 243–268.
[24] Mokry, P., Fukada, E., and Yamamoto, K., 2003, "Sound Absorbing System as an Application of the Active Elasticity Control Technique," J. Appl. Phys., **94**(11), pp. 7356–7362.
[25] Airoldi, L., and Ruzzene, M., 2011, "Design of Tunable Acoustic Metamaterials Through Periodic Arrays of Resonant Shunted Piezos," New J. Phys., **13**(11), p. 113010.
[26] Deü, J. F., Larbi, W., Ohayon, R., and Sampaio, R., 2014, "Piezoelectric Shunt Vibration Damping of Structural-Acoustic Systems: Finite Element Formulation and Reduced-Order Model," ASME J. Vib. Acoust., **136**(3), p. 031007.
[27] Chen, S. B., Wen, J. H., Yu, D. L., Wang, G., and Wen, X. S., 2011, "Band Gap Control of Phononic Beam With Negative Capacitance Piezoelectric Shunt," Chin. Phys. B, **20**(1), p. 014301.
[28] Akl, W., and Baz, A., 2013, "Active Acoustic Metamaterial With Simultaneously Programmable Density and Bulk Modulus," ASME J. Vib. Acoust., **135**(3), p. 031001.
[29] Behrens, S., Fleming, A. J., and Moheimani, S. R., 2003, "A Broadband Controller for Shunt Piezoelectric Damping of Structural Vibration," Smart Mater. Struct., **12**(1), pp. 18–28.
[30] Park, C., and Park, H., 2003, "Multiple-Mode Structural Vibration Control Using Negative Capacitive Shunt Damping," J. Mech. Sci. Technol., **17**(11), pp. 1650–1658.
[31] Beck, B., Cunefare, K., Ruzzene, M., and Collet, M., 2011, "Experimental Analysis of a Cantilever Beam With a Shunted Piezoelectric Periodic Array," J. Intell. Mater. Syst. Struct., **22**(11), pp. 1177–1187.
[32] Date, M., Kutani, M., and Sakai, S., 2000, "Electrically Controlled Elasticity Utilizing Piezoelectric Coupling," J. Appl. Phys., **87**(2), pp. 863–868.
[33] Imoto, K., Nishiura, M., Yamamoto, K., Date, M., Fukuda, E., and Tajitsu, Y., 2005, "Elasticity Control of Piezoelectric Lead Zirconate Titanate (PZT) Materials Using Negative-Capacitance Circuits," Jpn. J. Appl. Phys., **44**(9B), pp. 7019–7023.
[34] Zhu, R., Huang, G. L., Huang, H. H., and Sun, C. T., 2011, "Experimental and Numerical Study of Guided Wave Propagation in a Thin Metamaterial Plate," Phys. Lett. A, **375**(30–31), pp. 2863–2867.